Finite-bias charge detection in a quantum dot

R. Schleser, E. Ruh, T. Ihn, and K. Ensslin
Solid State Physics Laboratory, ETH Zürich, 8093 Zürich, Switzerland

D. C. Driscoll and A. C. Gossard
Materials Department, University of California, Santa Barbara, Santa Barbara, California 93106, USA
(Received 21 October 2004; revised manuscript received 3 May 2005; published 6 July 2005)

We present measurements on a quantum dot coupled capacitively to a quantum point contact used as a charge detector. The transport current through the dot and the time-averaged charge on the dot are measured simultaneously. At finite bias voltage through the dot, the differential charge signal coincides with some of the Coulomb diamond boundaries and with the signatures from excited states in the dot current. Combining the resulting integrated charge data with the simultaneous measurements of the dot current allows us to estimate the coupling of different energy levels inside the dot to both leads individually.

DOI: 10.1103/PhysRevB.72.035312 PACS number(s): 73.21.La, 73.23.Hk

I. INTRODUCTION

The charge state of a quantum dot can be read out using a nearby quantum point contact (QPC) as a detector.[1] Real time readout has been recently demonstrated using radio frequency single electron transistors[2] or QPCs.[3,4] Together with a spin-charge conversion mechanism, this is being considered a candidate for a qubit readout scheme[4] in a future quantum computing device based on coupled quantum dots.[5]

It is valuable to know how a quantum dot couples to each of the reservoirs. This coupling is determined by the electrostatic barrier forming the constriction and the wave function overlap leading to tunneling. The latter may strongly depend on the quantum state under consideration in the dot, which means that the quantum mechanical tunnel coupling has to be determined for each state individually. In the Coulomb blockade regime, for the case of single-level transport, a fit of a transport peak in the Coulomb blockade regime enables one to extract an effective tunnel coupling $\Gamma_{\mathrm{eff}} \equiv \Gamma_S \Gamma_D / (\Gamma_S + \Gamma_D)$, where Γ_S and Γ_D are the couplings to the source and the drain reservoir, respectively. However, the ratio Γ_S / Γ_D remains unknown.

In earlier work on finite bias transport,[6] e.g., in carbon nanotubes,[7] it was shown that, in principle, the individual coupling to both leads of the dot can be extracted from the current amplitudes at positive and negative bias. However, because these considerations make use of a spin blockade effect, they apply only to the case of spin degenerate states in the dot and require an even number of electrons on the dot. In addition, they rely on the absence of cotunneling. Recently, a method was presented[8] to measure the coupling of a dot to its reservoirs for a three-terminal quantum dot.

In the following, we present finite bias measurements of transport through a quantum dot, complemented by simultaneous measurements of the conductance of a nearby, electrostatically coupled QPC used as a charge detector. The latter allows us to determine the time-averaged charge on the quantum dot even in the nonblockaded regime, and the combination of both methods makes it possible to provide qualitative estimates for the quantum mechanical coupling of the dot's energy levels to each of the two reservoirs.

In these two sections, qualitative and quantitative information about the coupling of several single-particle levels to both leads is extracted. This is done by comparison of experimental data to both analytical and numerical simulations, using a sequential-tunneling model.[9]

II. EXPERIMENTAL SETUP

The sample [see Fig. 1(a)] was fabricated using surface probe lithography[10–12] on a $GaAs/Al_{0.3}Ga_{0.7}As$ heterostructure, containing a two-dimensional electron gas (2DEG) 34 nm below the surface as well as a backgate (BG) 1400 nm below the 2DEG. The unstructured 2DEG had a mobility of $(3.5 \pm 0.5) \times 10^5$ cm^2/V s and an electron density 4.6×10^{11} cm^{-2} at a BG voltage $V_{\mathrm{BG}} = -0.5$ V at $T = 4.2$ K.

All measurements were performed in a dilution refrigerator at a base temperature of 80 mK.

Negative voltages were applied to the surrounding gates [G1, G2, S_{QPC}, D_{QPC}, the latter two also containing the charge detection circuit; see Fig. 1(a)], and to the BG, to reduce the charge on the dot and close its tunnel barriers. A voltage applied to gate P was used to tune the detector QPC to a regime where it is sensitive to the charge on the dot. The quantum dot (QD) bias voltage was applied symmetrically (with respect to ground) across the dot between source (S_{QD}) and drain (D_{QD}).

Due to the electrostatic coupling of the QPC to the dot, a change in the dot's charge leads to a modification in the QPC's confining potential, resulting in a change of its conductance.[1] The latter was measured by applying a dc voltage and measuring the resulting current. Each additional electron on the dot leads via electrostatic interaction to a shift of the QPC conductance's dependence on gate voltage: $I_{\mathrm{qpc},N}(V_{\mathrm{gate}}) = I_{\mathrm{qpc},N+1}(V_{\mathrm{gate}} + \Delta V)$, where N is the number of electrons on the dot. If we assume that the QPC is tuned to a regime between two conductance plateaux with an approximately constant derivative $dI_{\mathrm{qpc}}/dV_{\mathrm{gate}}$, then we can subtract $I_{\mathrm{qpc},N=\mathrm{const}}(V_{\mathrm{gate}})$ as a background and get a signal proportional to the additional charge on the dot: $Q \propto I_{\mathrm{qpc}}(V_{\mathrm{gate}})$

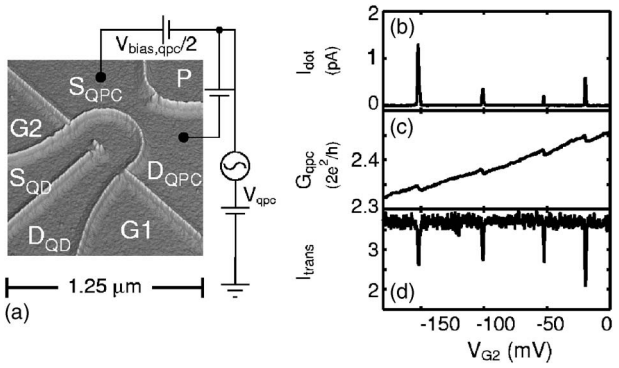

FIG. 1. (a) Atomic force microscopy (AFM) micrograph of the structure with designations of gates: source (*S*) and drain (*D*) of the QD and the QPC used as a charge detector; lateral gates G1 and G2 to control the coupling of the dots to the reservoirs; plunger (*P*) gate to tune the QPC detector. Only the part of the circuit related to the readout functionality is included. V_{qpc} consists of a dc and a small ac component ($V_{\mathrm{qpc,ac}} \leqslant 5\ \mu$V). (b) Example measurement of the current through the dot. For these low bias measurements, the voltage across the dot was $V_{\mathrm{bias,dot}}=10\ \mu$V. (c) Simultaneous measurement of the conductance through the QPC, where each step corresponds to a change of the dot's charge by one electron. (d) Simultaneous measurement of the transconductance $dI_{\mathrm{qpc}}/dV_{\mathrm{qpc}}$.

$-I_{\mathrm{qpc},N=\mathrm{const}}(V_{\mathrm{gate}})$. This technique has recently been applied to investigate the charging behavior of a double quantum dot.[13]

In our measurements, to avoid the influence of nonmonotonuous drift in I_{qpc}, we measured the transconductance $dI_{\mathrm{qpc}}/dV_{\mathrm{qpc}}$ as an additional quantity, using a lock-in setup at a frequency of $f=31$ Hz. The voltage V_{qpc} was composed of a constant dc voltage, used to tune both the dot's and the QPC's chemical potential, and a small ac voltage used to periodically change the chemical potential inside the dot by a small amount (of the order of k_BT). The bias $V_{\mathrm{bias,qpc}}$ across the QPC was applied symmetrically with respect to V_{qpc} to minimize its influence on the chemical potential inside the dot. Figure 1(a) illustrates the QPC related part of the circuit diagram. Figures 1(b)–1(d) show the correlations between the three quantities in a simultaneous measurement: at the position of a Coulomb blockade peak in the current through the dot, a kink appears in the QPC's conductance, corresponding to a change in the dot's charge by one. In the transconductance $dI_{\mathrm{qpc}}/dV_{\mathrm{qpc}}$, a dip is observed. The transconductance $dI_{\mathrm{qpc}}/dV_{\mathrm{qpc}}$, being a derivative of the QPC current, differs from $dI_{\mathrm{qpc}}/dV_{\mathrm{G2}}$ only by a constant background and a factor given by the ratio of the corresponding lever arms, $\alpha_{\mathrm{G2}}/\alpha_{\mathrm{qpc}}$. This ratio should depend only weakly on gate voltages. One can therefore obtain the time-averaged charge on the dot by integrating the measured value $dI_{\mathrm{qpc}}/dV_{\mathrm{qpc}}$ with respect to V_{G2} and normalizing the resulting steps to unity.

III. TIME-AVERAGED CHARGE DETECTION

In Fig. 2(a), we present finite bias measurements of the dot's conductance. From these, estimates for the charging energy $E_c \approx 1.6$ meV and the mean level spacing $\Delta \approx 300\ \mu$eV were extracted. Figure 2(b) shows a simultaneous measurement of the QPC's transconductance.

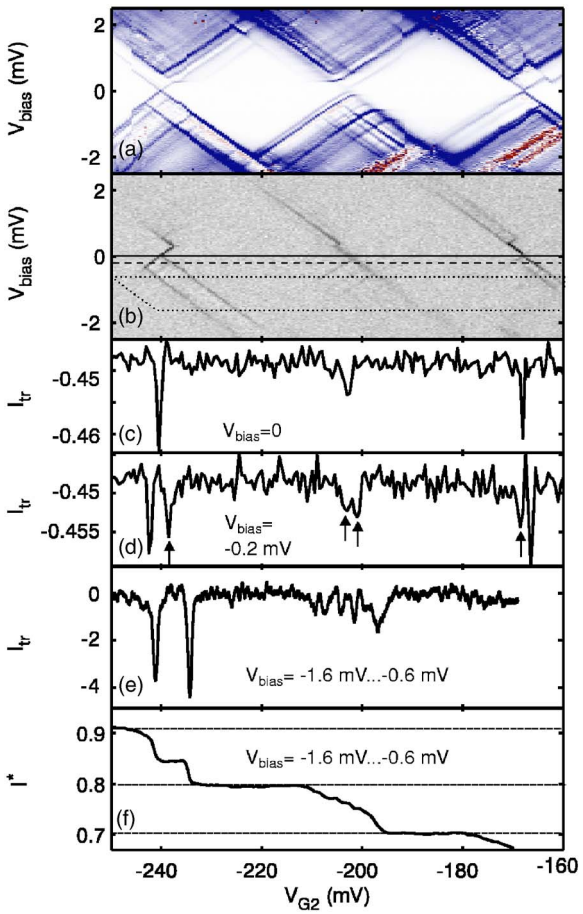

FIG. 2. (Color online) (a) Finite bias transport measurement through the dot at a magnetic field of $B=0.1$ T. Dark regions represent larger positive (blue) or negative (red) differential conductance. (b) Corresponding measurement of the transconductance. Dark regions represent more negative values. (c) Single transconductance trace for low bias [$V_{\mathrm{bias}}=20\ \mu$V, see the upper horizontal line in (b)]. (d) Single transconductance trace for $V_{\mathrm{bias}}=-0.2$ mV [see the dashed horizontal line in (b)]. (e) Averaged transconductance. Averaging was performed over a set of bias voltages $-1.6\ \mathrm{mV} < V_{\mathrm{bias}} < -0.6$ mV. Individual traces were laterally shifted with respect to each other so that the two lines visible in the lower left part of (b) [parallel to the diamond edges in (a)] yield two distinct sharp peaks. The region delimited by dotted lines in (b) marks the range over which averaging took place. As a consequence, the step corresponding to the second Coulomb peak is broadened, because for this peak the slope of the corresponding lines in (b) is different. A constant and a linear background were subtracted. (f) Averaged transconductance integrated with respect to V_{G2}.

In the transconductance plot, diagonal lines with the same slope as the diamond boundaries in the dot conductance plot are observed, marking a change of the dot's time-averaged charge. The lines correspond to the alignment of an energy level in the dot with either the source (negative slope) or the drain (positive slope) reservoir, and their intensity contains information about the magnitude of the change in charge.

Figure 2(c) shows the transconductance at low bias. Dips in the signal at the gate voltages of the Coulomb blockade peaks correspond to the change in electronic charge by one elementary charge each. For a finite bias $V_{\mathrm{bias}}=-0.2$ mV [Fig. 2(d)], the peaks split, illustrating that the time-averaged charge on the dot changes in steps smaller than the unit charge e.

These steps in charge can be directly visualized by integrating over the transconductance [Figs. 2(e) and 2(f)]. To improve the precision of the charge determination, the transconductance was averaged over a finite bias range prior to numerical integration. A constant (corresponding to the direct coupling between the in-plane gates used for ac excitation and the QPC) and a linear term (corresponding to the gate voltage dependence of $\alpha_{\mathrm{G2}}/\alpha_{\mathrm{qpc}}$) were then subtracted.

The large steps marked by dashed horizontal lines in Fig. 2(f), corresponding to a change in charge by one elementary charge each, have almost identical height, as one would expect. Charge rearrangements during the measurements, one of which is visible at $V_{\mathrm{G2}}\approx 235$ mV in Fig. 2(a), might contribute to errors in the numerical integration and thus may lead to small differences in the total step height.

To verify the usefulness of the integrated signal as a measure for the mean charge on the dot, we compared the step size related to a single electronic charge for several Coulomb peaks [see Fig. 2(f)] and for different bias ranges. The difference in step height did not exceed 10% if a sufficient number of traces was taken into account to reduce the statistical error. Even in the high bias regime $1.2\ \mathrm{mV}<V_{\mathrm{bias}}<1.6$ mV near the border of the Coulomb blockaded bias range, where the lines in the transconductance seem to gradually disappear, the integrated transconductance signal gives a good measure of the mean charge.

IV. ESTIMATION OF DOT-LEAD COUPLING: NONDEGENERATE CASE

From the information about the mean charge in the nonblockaded region, it is possible to extract the coupling of individual states to each lead separately by using a rate equation approach.[9] If a single energy level lies within the bias range between the Fermi level of both leads, the mean dwell time of the Nth electron in the dot is determined by the relative value of the couplings $\Gamma_{\mathrm{S},N}$ and $\Gamma_{\mathrm{D},N}$ to both leads. The $\Gamma_{\mathrm{i},N}$'s account for the height of the tunnel barriers i, the wave function overlap between the dot and lead, and the density of states inside the leads, which we assume to be constant. The occupation probability of the energy level N then becomes

$$P(N)=\frac{\Gamma_{\mathrm{S},N}f_{\mathrm{S}}(\mu_N)+\Gamma_{\mathrm{D},N}f_{\mathrm{D}}(\mu_N)}{\Gamma_{\mathrm{S},N}+\Gamma_{\mathrm{D},N}}, \tag{1}$$

where f stands for the energy distribution in the leads (which we assume to be the Fermi distribution) and the indices "S" and "D" stand for source and drain, respectively. For a bias voltage $|V_{\mathrm{bias}}|=|E_{\mathrm{F,S}}-E_{\mathrm{F,D}}|\gg k_{\mathrm{B}}T$ and a chemical potential μ_N not inside the thermally broadened ranges around the Fermi energies of both leads, we have $f_{\mathrm{S}}(\mu_N)=1$, $f_{\mathrm{D}}(\mu_N)=0$, and this expression becomes $P^{+}(N)=\Gamma_{\mathrm{S},N}/(\Gamma_{\mathrm{S},N}+\Gamma_{\mathrm{D},N})$ for $E_{\mathrm{F,S}}>E_{\mathrm{F,D}}$ (positive bias) and $P^{-}(N)=\Gamma_{\mathrm{D},N}/(\Gamma_{\mathrm{S},N}+\Gamma_{\mathrm{D},N})$ for $E_{\mathrm{F,S}}<E_{\mathrm{F,D}}$ (negative bias).

Because the noninteger (fluctuating) part of the mean charge on the dot in the level N is given by $eP^{\pm}(N)$, this connects the integrated transconductance value to the ratio $\Gamma_{\mathrm{S},N}/\Gamma_{\mathrm{D},N}$:

$$\frac{\Gamma_{\mathrm{S},N}}{\Gamma_{\mathrm{D},N}}=\frac{P^{+}(N)}{P^{-}(N)}=\frac{P^{+}(N)}{1-P^{+}(N)}. \tag{2}$$

Together with the expression for the transport current

$$I=-e\frac{\Gamma_{\mathrm{S},N}\Gamma_{\mathrm{D},N}}{\Gamma_{\mathrm{S},N}+\Gamma_{\mathrm{D},N}}, \tag{3}$$

it is possible to determine the numerical values of $\Gamma_{\mathrm{S},N}$ and $\Gamma_{\mathrm{D},N}$.

The analysis of the transconductance signal becomes more involved if more energy levels inside the quantum dot are contributing to transport. It is thus preferable to start the analysis in the regime of single-level transport, i.e., $V_{\mathrm{bias}}<(\Delta-k_{\mathrm{B}}T)$. In addition, the maxima in the transconductance signal associated with source and drain alignment of the level must be clearly separable, i.e., $V_{\mathrm{bias}}>k_{\mathrm{B}}T$. Those two requirements limit the bias range over which the integration of the transconductance peak can be performed on a given data set, especially when excited states are present near the ground state. To apply the method described above, we have to verify that there exists a finite bias range where these conditions are met.

We analyzed the low finite bias regime around three conductance peaks in a range where the system was most stable, for five different magnetic fields applied, to change the shape of the dot's wave functions and their overlap with the leads. In our analysis, we encounter two qualitatively different situations in the low bias transconductance regime. (i) No branching at zero bias (this section): single line with constant slope crossing the zero bias line, possibly branching at finite bias. (ii) Branching at zero bias (degenerate case, discussed in Sec. V).

An example of the first case is encountered, e.g., at the second peak in Figs. 2(a) and 2(b) [see detail in Fig. 3(a)], in the low bias regime: near $V_{\mathrm{bias}}=0$, we observe a broadened line with negative slope in the transconductance, while a similarly broadened, but comparatively weak maximum is measured in the transport current [Fig. 2(a)].

Figure 3(b) shows a schematic representation of Fig. 3(a), illustrating which line corresponds to the alignment of the dot's chemical potential with source (S) and drain (D). Figures 3(c)–3(f) illustrate how coupling and level alignment determine the mean electron number on the dot. Note that in Fig. 3(e), an asymmetrically coupled level can become nearly 100% occupied even in the nonblockaded regime.

The observation near $V_{\mathrm{bias}}=0$ is compatible with the presence of a single energy level strongly coupled to the source reservoir (leading to enhanced broadening, compared to a Coulomb blockade peak width of purely thermal origin), but extremely weakly coupled to the drain contact. This would explain the observed low zero bias transport current and the

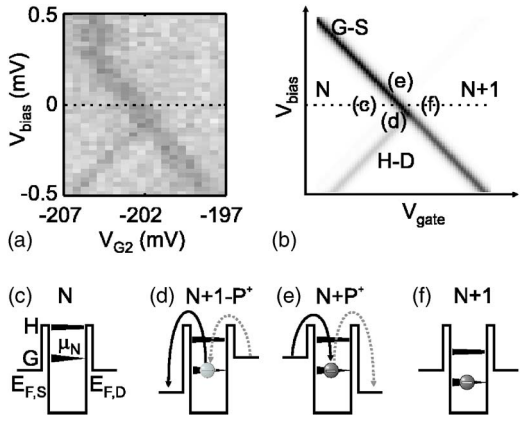

FIG. 3. (a) Detail from Fig. 2(b), showing a broadened line with negative slope at zero bias and a splitting at finite bias. (b) Illustration of the connection between the coupling of a single state (G) to source (S) and drain (D) and the mean charge on the dot. This representation was generated using a simulation based on a rate equation approach (Ref. 9), and is compatible with our experimental observations (with the exception of line broadening due to strong coupling, which is not included in the theory). Our model for this case includes two single-particle levels: an asymmetrically coupled state accounting for the imbalance of line weight observed at positive and low negative bias (where the line with positive slope, corresponding to alignment of G with D, is practically absent), and a higher energy level H with more symmetric coupling, responsible for the branching at finite negative bias. We used coupling asymmetries $\Gamma_{D,G}/\Gamma_{S,G}=1/50$ for the level G, and $\Gamma_{D,H}/\Gamma_{S,H}=1/4$ for the level H. In additon, we set $\Gamma_{D,G}+\Gamma_{S,G}=\Gamma_{D,H}+\Gamma_{S,H}$. The diagonal line ($G$-$S$) with negative slope corresponds to the alignment of a single energy level (G) with the source (S) contact, and the line (H-D) with positive slope in the negative bias range marks an alignment of an excited state (H) with the drain (D) contact. Letters in parentheses [(c)–(f) located in the blockaded (left and right) and nonblockaded (top and bottom) regions] refer to the corresponding figures. These illustrate how the time-averaged electron number depends on the bias and the chemical potential of the dot for the case of an asymmetric (here $P^+>1/2$) coupling.

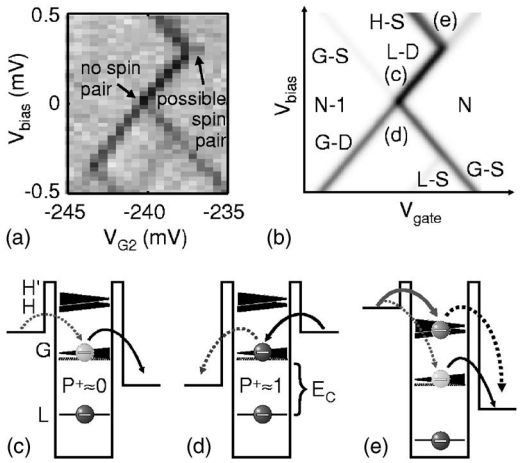

FIG. 4. (a) Detail from 2(b), showing discontinuity (splitting) of lines in the transconductance signal at zero bias. (b) Schematic representation of (a) generated by a numerical simulations. To explain the observed line splitting, a simplified model spectrum with four states is used, consisting of two pairs of (quasi)degenerate levels. Small letters in parentheses refer to (c)–(e), where the spectrum is depicted for different values of gate and bias voltage, illustrating how the interplay of several levels with different couplings to the leads influences the time-averaged occupation of the dot. The labeled lines in (b) refer to the alignment of a level [L,G, or H/H', see (c)] with either source (S) or drain (D). (c) For low positive bias, charge passes through the degenerate levels G and L. Due to the asymmetric coupling, the mean charge remains low until alignment with the drain contact. (d) For small negative bias, the asymmetry in the coupling of levels L and G leads to a finite mean charge on the dot as soon as they align with the drain's chemical potential [see line G-D in (b)]. (e) In this parameter range, the mean charge reaches a high level, due to the asymmetric coupling of the levels H and H' that trap charge entering through the source contact.

fact that within our measurement resolution, no line with positive slope corresponding to an alignment to the drain contact is observed in the transconductance. At finite negative bias, i.e., once a more symmetrically coupled excited state becomes accessible [see the finite bias region around middle peak in Fig. 2(a)], transport is strongly enhanced.

Solving Eqs. (1) and (3) for $\Gamma_{S,N}$ and $\Gamma_{D,N}$ yields an upper bound for the ratio of the coupling constants $\Gamma_{D,N}/\Gamma_{S,N} \leqslant 1/50$. From the measured value of the transport current in the finite bias regime (averaged over positive and negative bias), we obtain an estimate for $\Gamma_{S,N}\Gamma_{D,N}/(\Gamma_{S,N}+\Gamma_{D,N})$, so that both are uniquely determined within the errors resulting from charge measurement uncertainties. In fact, for this very asymmetric case, we might assume that level broadening is caused entirely by the more strongly coupled source lead. The full width at half maximum of the Coulomb peak is of the order $w_{\mathrm{FWHM}}=130\ \mu\mathrm{eV}<\Delta$, yielding a value for $\Gamma_{S,N}$, which suggests an even stronger asymmetry $\Gamma_{D,N}/\Gamma_{S,N} \leqslant 1/1000$.

At finite bias, a splitting of the line in the transconductance is observed, suggesting that an excited state of the dot more symmetrically coupled to both leads governs its mean occupation. Inserting this into a numerical simulation (see below) also yields qualitative agreement with the observed finite bias dot current, which shows a larger step change at the positive than at the negative bias corresponding to the excitation energy.

V. ESTIMATION OF DOT-LEAD COUPLING: DEGENERATE CASE

In a number of cases the lines in the transconductance plot branch at zero bias [leftmost peak in Fig. 2(b), see detail in Fig. 4(a)]. This splitting is not compatible with the participation of only one individual single-particle level in transport.

From our transconductance measurements, the mean occupation was determined by integrating over a voltage range in V_{G2} in the transconductance plot, summing over a range of bias voltages to reduce the statistical errors. Normalization was performed by integrating over the whole nonblockaded gate voltage range, summing over the same bias range.

To elucidate the origin of the low bias results [depicted schematically in Fig. 4(b)], we performed analytical calculations using a rate equation approach based on the framework

of Beenakker's theory of sequential electron tunneling.[9]

We assumed that a model involving at least two quasidegenerate states might describe our findings, and therefore extended Eqs. (1)–(3) to the case of two degenerate levels, involving four coupling values $\Gamma_{i,j}$ ($i=S,D$ for source and drain; $j=1, 2$).

To extract a meaningful result despite the large relative errors in the charge input values, we express the $\Gamma_{i,j}$ in terms of a global multiplicative factor $\Gamma_0=\sqrt[4]{\Pi_{i,j}\Gamma_{i,j}}$, the symmetries of each of the two states $S_i=\sqrt{\Gamma_{S,i}/\Gamma_{D,i}}$ and the relative weight of the two states $V=\sqrt[4]{\Gamma_{S,1}\Gamma_{D,1}/\Gamma_{S,2}\Gamma_{D,2}}$, expressed as the ratio of the geometrical averages of their couplings. The resulting simple expressions for the $\Gamma_{i,j}$ become $\Gamma_{S,1}=\Gamma_0 VS_1$, $\Gamma_{D,1}=\Gamma_0 V/S_1$, $\Gamma_{S,2}=\Gamma_0 S_2/V$, $\Gamma_{D,2}=\Gamma_0/(VS_2)$.

Using the four charge and transport values at low positive and negative bias as input values, the expressions for current and occupation can be solved for the four new parameters. The numerical values obtained are $\hbar\Gamma_0=(2.0\pm0.7)\mu$eV, $V=1.23\pm0.50$, $S_1=1.10\pm0.15$, $S_2=0.22\pm0.12$. This means that one of the two levels has approximately symmetric coupling, and the second is predominantly coupled to the drain contact. However, from the majority of lines with negative slopes in Fig. 2(b), we learn that the dot as a whole is predominantly coupled to the source contact. This means that the second level has a strongly asymmetric wave function overlap, opposite to the asymmetry of the electrostatic tunnel barriers.

Because the numbers show that the two states have different symmetry properties, the most obvious possibility of a spin pair has to be excluded in this case.

The method described above can be extended to determine the coupling properties of higher energy states by incrementally solving the more intricate rate equations involving a larger number of levels, using measurements at higher bias and the previously calculated $\Gamma_{i,j}$ values as an input. The major advantage of this procedure is that it correlates data measured at a constant value of the controlling gate, changing only the bias of the dot: due to spectral scrambling, the information obtained in this way is rarely accessible by comparing successive Coulomb peaks.

We performed this advanced analysis using numerical calculations based on the same aforementioned rate equation approach. Even though the incremental nature of the procedure accumulates experimental errors from the current and charge measurements (see next paragraph), some qualitative statements can be derived: The most important one concerns the feature visible in Fig. 4(a), showing a change in slope in the right positive bias line occuring at finite bias. The fact that the line with a positive slope is discontinued is not compatible with the presence of a single excited state. Again, at least two quasidegenerate states are necessary to explain the scenario observed. The coupling of these two states has to be asymmetric with predominant coupling to the source contact. The measurements are compatible with the two states having identical coupling values, leaving open the possibility of a spin pair. Figure 4(b) shows a numerical simulation using the values $\Gamma_{i,j}$ from the analytical calculations above for the two lower states (responsible for the low bias behavior). The remaining $\Gamma_{i,j}$ were determined numerically by iteratively comparing experiment and simulation.

The resolution of our charge detector is limited: all the transconductance measurements presented above were performed in a regime in which the QPC's conductance remained between $2e^2/h$ and $4e^2/h$. Slight changes in the lithographic pattern for future structures will permit us to approach the tunneling regime in the QPC. Together with a higher resolution in gate voltage, this will result in a more than tenfold increase in charge sensitivity and a more precise determination of the average electronic charge and the coupling strengths.

VI. CONCLUSIONS

We have performed transport measurements on a quantum dot and, simultaneously, on a nearby quantum point contact used as a charge detector. Our measurements were carried out at finite dot bias and allow us to determine the noninteger time-averaged electronic charge on the dot in the nonblockaded regime.

Combining the information obtained from transport and charge measurements allows us, via a sequential tunneling model, to make quantitative statements about the relative occupation of individual single electron levels, and especially about the quantum mechanical coupling of these levels to both source and drain individually.

Although the present measurements serve as a proof of principle, future measurements will, by a few straightforward changes in the setup, allow for a huge increase in the numerical quality of our data. At the present level, however, our results already allow us to fine tune the asymmetry of the dot-lead coupling for specific applications.

ACKNOWLEDGMENT

Financial support from the Schweizerischer Nationalfonds is gratefully acknowledged.

[1] M. Field, C. G. Smith, M. Pepper, D. A. Ritchie, J. E. F. Frost, G. A. C. Jones, and D. G. Hasko, Phys. Rev. Lett. **70**, 1311 (1993).

[2] Wei-Lu, Zhongqing-Ji, L. Pfeiffer, K. W. West, and A. J. Rimberg, Nature (London) **423**, 422 (2003).

[3] R. Schleser, E. Ruh, T. Ihn, K. Ensslin, D. C. Driscoll, and A. C. Gossard, Appl. Phys. Lett. **85**, 2005 (2004).

[4] J. M. Elzerman, R. Hanson, L. H. W. van Beveren, B. Witkamp, L. M. K. Vandersypen, and L. P. Kouwenhoven, Nature (London) **430**, 431 (2004).

[5] D. Loss and D. P. DiVincenzo, Phys. Rev. A **57**, 120 (1998).

[6] E. Bonet, M. M. Deshmukh, and D. C. Ralph, Phys. Rev. B **65**, 045317 (2002).

[7] D. H. Cobden, M. Bockrath, P. L. McEuen, A. G. Rinzler, and R. E. Smalley, Phys. Rev. Lett. **81**, 681 (1998).

[8] R. Leturcq, D. Graf, T. Ihn, K. Ensslin, D. D. Driscoll, and A. C. Gossard, Europhys. Lett. **67**, 439 (2004).
[9] C. W. J. Beenakker, Phys. Rev. B **44**, 1646 (1991).
[10] R. Held, S. Lüscher, T. Heinzel, K. Ensslin, and W. Wegscheider, Appl. Phys. Lett. **75**, 1134 (1999).
[11] S. Lüscher, A. Fuhrer, R. Held, T. Heinzel, K. Ensslin, and W. Wegscheider, Appl. Phys. Lett. **75**, 2452 (1999).
[12] R. Nemutudi, M. Kataoka, C. J. B. Ford, N. J. Appleyard, M. Pepper, D. A. Ritchie, and G. A. C. Jones, J. Appl. Phys. **95**, 2557 (2004).
[13] L. DiCarlo, H. J. Lynch, A. C. Johnson, L. I. Childress, K. Crockett, C. M. Marcus, M. P. Hanson, and A. C. Gossard, Phys. Rev. Lett. **92**, 226801 (2004).